Available online at www.sciencedirect.com
SCIENCE DIRECT
Sensors and Actuators A 128 (2006) 333–338
SENSORS AND ACTUATORS A PHYSICAL
www.elsevier.com/locate/sna

Color aliasing free thin-film sensor array

Dietmar Knipp [a,c,*], Robert A. Street [a], Helmut Stiebig [b], Mathias Krause [b,1], Jeng-Ping Lu [a], Steve Ready [a], Jackson Ho [a]

[a] *Palo Alto Research Center, Electronic Materials and Devices Laboratory, Palo Alto, CA 94304, USA*
[b] *Research Center Jülich, Institute of Photovoltaics, 52425 Jülich, Germany*
[c] *International University Bremen, Department of Science and Engineering, 28759 Bremen, Germany*

Received 22 July 2005; received in revised form 16 January 2006; accepted 2 February 2006
Available online 13 March 2006

Abstract

Color information and color images are commonly captured by sensor arrays in combination with optical filters. However, the detection of the fundamental colors red, green and blue at different spatial positions of the sensors array leads to color aliasing or color moiré effects. This limitation is inherent to conventional sensor arrays using optical filters. To overcome this limitation color sensors based on vertically integrated thin-film structures were realized. The complete color information is detected at the same position of a sensor array without using optical filters. The sensors consist of an amorphous silicon 'nipiin'-structure. The spectral sensitivity of the sensors is controlled by the applied bias voltage. The three-color sensors were integrated on top of an amorphous silicon readout electronic. The operating principle of the color sensor will be described and the performance of the color aliasing free sensor in terms of spectral sensitivity and pixel cross-talk will be discussed in this paper.

Keywords: Optical sensor; Color sensor; Sensor array; Amorphous silicon; Thin-film transistors; TFTs

1. Introduction

Imaging is usually performed by silicon sensor arrays in combination with color filter arrays (CFA). Color filter arrays consist of a spatial arrangement of at least three filters for the colors red, green and blue. However, color detection using CFAs leads to color moiré or color aliasing effects as the different colors are detected at spatial different positions [1]. Furthermore, the spatial resolution of conventional sensor arrays is limited as three chromatic color pixels are required.

In order to overcome the color moiré effect, vertically integrated sensor structures were proposed and developed. These structures detect the color information in the depth of the device. Due to the wavelength dependent absorption of the applied semiconductor materials, photons are absorbed in various depths of the device. High energetic photons are absorbed close to the surface of the detector, whereas low energetic photons penetrate deeper in the material. A comparison of a sensor arrays using a Bayer color filter array and a vertically integrated color sensor is shown in Fig. 1. To illustrate the operation principle of a color moiré or color aliasing free sensor an edge was projected on both of the sensor structures. Due to the finite size of the sensor pixels aliasing effects are observed for both structures. However, for the vertically integrated sensor only black and white aliasing is observed, whereas for the sensor using a color filter array black and white aliasing plus color aliasing is observed. The influence of the color aliasing effect on the reconstructed image is shown in Fig. 1c. The colors detected at the edges of the projected image are distorted. In the case of a black and white edge projected on the sensors the CFA based sensor even detects colors even though the projected image is colorless.

Various vertically integrated sensor structures have been realized by using different materials, design concepts and contact configurations [1–10]. The suggested sensors range from two terminal devices, which change their spectral sensitivity by varying the applied bias voltage to vertically stacked diodes.

Vertically integrated color sensor arrays have been demonstrated by Lyon and Hubel [1], Schneider et al. [11] and Theil [12]. The structures realized by Hubel and coworkers consist of three vertically integrated 'pn'-junctions fabricated by standard silicon BiCMOS technology. Sensor arrays with a resolution of

* Corresponding author.
E-mail address: d.knipp@iu-bremen.de (D. Knipp).
[1] Present address: Infineon Technology, Dresden, Germany.

0924-4247/$ – see front matter © 2006 Elsevier B.V. All rights reserved.
doi:10.1016/j.sna.2006.02.007

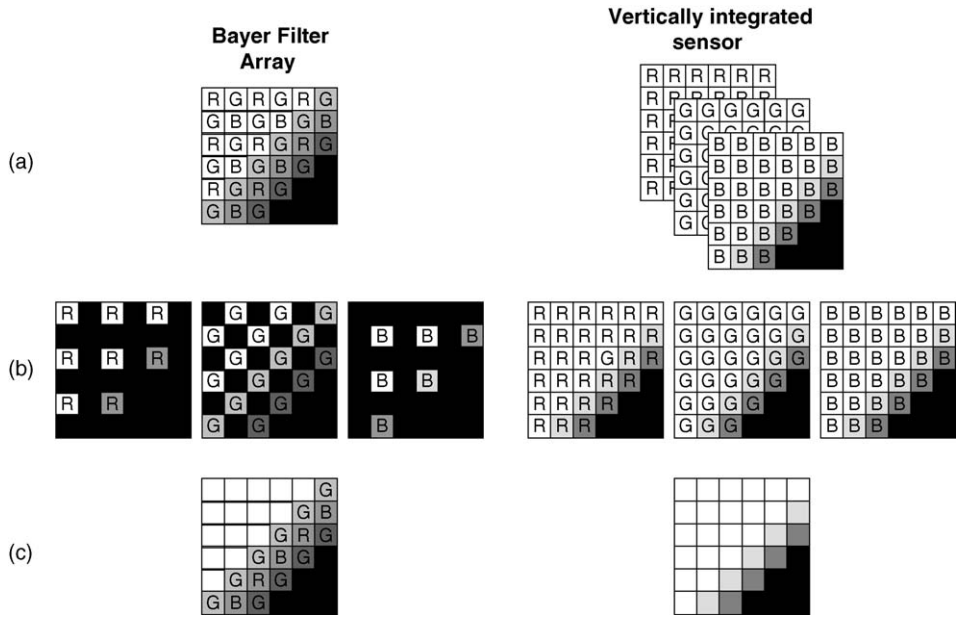

Fig. 1. Schematically illustrated edge detection of a sensor using a color filter array and a vertically integrated sensor. (a) A black and white image of an edge is projected on the color filter array and the vertically integrated sensor; (b) R, G and B images of the projected image; (c) resulting image of the projected edge.

10.6 Mpixels were realized [1]. The metameric color error of the sensors is comparable to standard image sensors using color filter arrays. Schneider et al. [11] and Theil [12] presented an approach, where amorphous silicon based color sensors were integrated on top of a CMOS readout electronic. The integration of the sensor on top of a readout electronic prevents color moiré effects and facilitates the realization of sensor arrays with high area fill factors.

So far large area sensor arrays using vertically integrated sensors have not been presented even though such sensor arrays are of interest for a variety of applications. In particular those applications are of interest, where the requirements in terms of cost and scalability are different from classical silicon microelectronics. Typical examples are large area scanners or other sensor applications, where the sensor array is used as a platform for a Lab-on-Chip system.

In this paper, we present sensors which consist of amorphous silicon two terminal devices in combination with amorphous silicon thin-film transistor technology. The entire sensor array is realized on a glass substrate at low deposition temperatures using a plasma enhanced chemical vapor deposition (PECVD) process. In the first part of the paper, the sensor concept and the fabrication of the sensor array will be described. In the second part, the performance of the sensor array in terms of spectral sensitivity and pixel cross-talk will be discussed.

2. Experiment

The sensor arrays were fabricated by plasma enhanced chemical vapor deposition at temperatures below 300 °C on 4-in. glass wafers. A cross-section of a sensor pixel of the sensor arrays is shown in Fig. 2.

The optical sensor is integrated on top of the readout electronic to achieve a high area fill factor. The sensor array has a resolution of 512×512 pixels and a pixel pitch of $100\,\mu m \times 100\,\mu m$. Pixel addressing is realized by amorphous silicon thin-film transistors (TFTs). Each pixel contains a top gate TFT, a storage capacitor, address and data lines, and a contact pad to the sensor occupying 67% of the pixel area. A detailed description of the deposition parameters and the device performance of the amorphous silicon thin-film transistor are given elsewhere [13]. A pixel circuit of the sensor array is given in Fig. 3.

The actual color sensor itself is realized by an anti serial connection of two amorphous silicon pin diodes. To planarize the underlying readout electronic and to reduce the coupling between the optical sensor and the readout electronics a 3–10 μm thick oxynitride layer was prepared by PECVD on top of the readout transistors. Only the back contact and the 'n'-layer of the optical sensors were patterned. The remaining layers of the optical sensor and the top electrode of the sensor array were unpatterned as illustrated in Fig. 2. The sensor consists of a multi layer stack of amorphous silicon and amorphous silicon

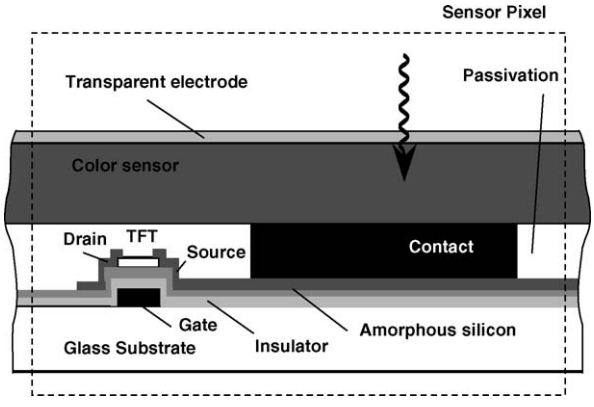

Fig. 2. Cross-section of a pixel of a large area color sensor array.

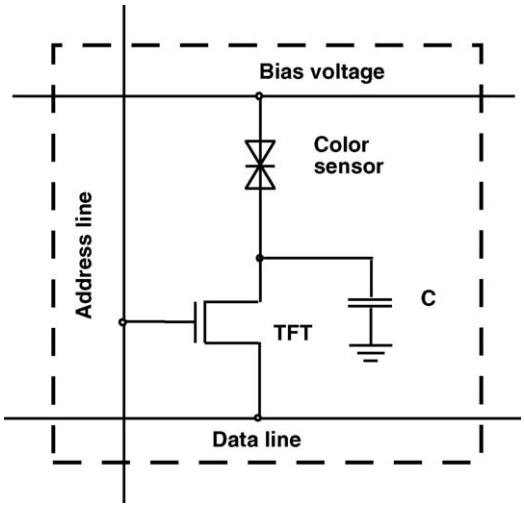

Fig. 3. Pixel circuit of a pixel of a large area three-color sensor array.

carbon layers. A description of the deposition parameters of the amorphous silicon films is given in reference [16]. The top contact of the sensor array was realized by a doped zinc oxide layer, which was sputtered on top of the amorphous silicon stack [14].

3. Results

3.1. Operating principle of the color sensor

To minimize the color error of the three-color sensor the spectral sensitivities have to be matched to the color space of the human eye represented by the colorimetric standard observer (CIE 1931) [15]. Therefore, bandgap engineering of the individual regions of the sensor is need to optimize the spectral sensitivities. The bandgap diagram of the optical sensor under thermal equilibrium is shown in Fig. 4a.

The top diode, which is firstly penetrated by the incoming light, is realized by a wide bandgap silicon carbon absorber. The absorber in the top diode ('i_I'-layer) has an optical bandgap of 2.2 eV and a thickness of 85 nm. Therefore, blue light is absorbed in the top diode, whereas green and red light is transmitted through the top diode.

The absorber of the bottom diode is divided in two regions. Region 'i_{II}' of the bottom diode was realized by a silicon carbon layer with an optical bandgap of 1.9 eV, whereas the region 'i_{III}' was formed by an intrinsic amorphous silicon layer. The 'i_{II}'- and 'i_{III}'-layers have a thickness of 145 and 365 nm. A summary of the deposition conditions of the sensor structure is given in Table 1.

The optical generation rate within the individual regions of the sensor is illustrated in Fig. 5. The optical generation rate within sensor structure was calculated by

$$G(\lambda, x) = \phi_0 \cdot \alpha(\lambda, x) \cdot \exp(-\alpha(\lambda, x) \cdot x), \quad (1)$$

Table 1
Deposition parameters of the three-color 'nipiin'-sensor

Function	Material	Bandgap [eV]	Thickness [nm]
TCO	ZnO	–	500
'n'-layer	a-Si:H	1.74	15
'i'-layer	a-SiC:H	2.2	85
'p'-layer	a-SiC:H	1.9	30
'i'-layer	a-SiC:H	1.9	145
'i'-layer	a-Si:H	1.74	365
'n'-layer	a-Si:H	1.74	30
Metal	Cr	–	–

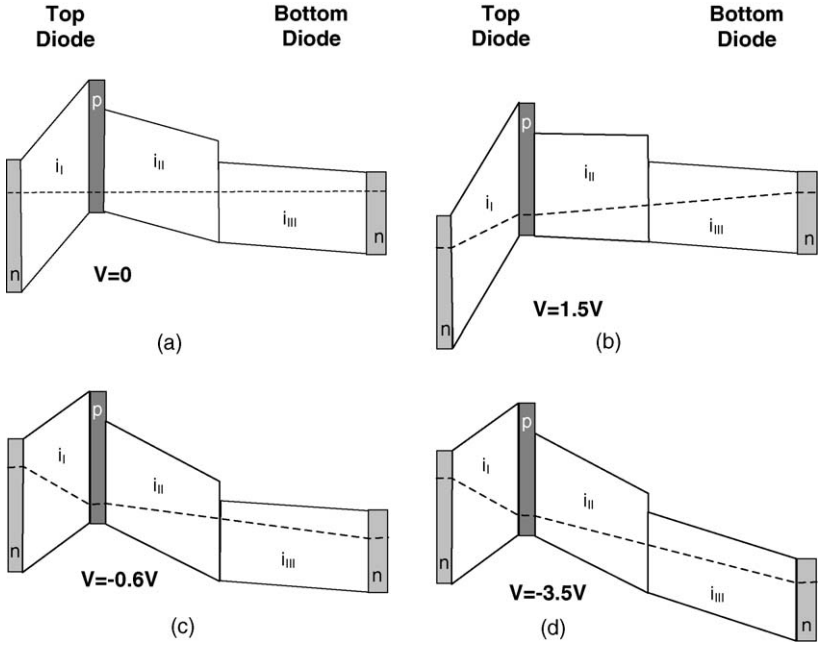

Fig. 4. Schematic band structure of the 'nipiin'-sensor under thermal equilibrium (a), and under applied bias voltages of: +1.5 V (b), −0.6 V (c) and −3.5 V (d).

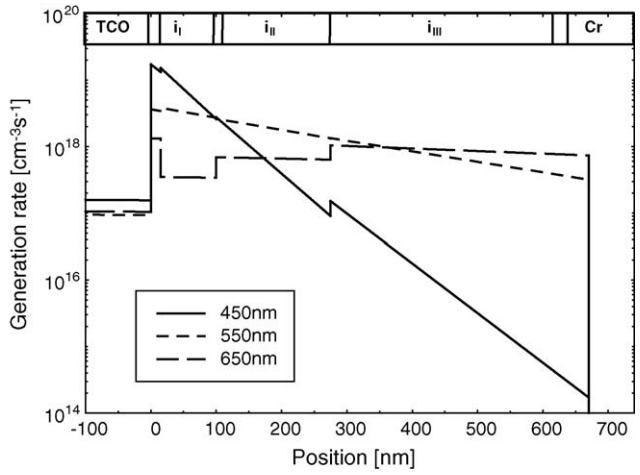

Fig. 5. Optical generation rate within the sensor structure for a given photon flux of 10^{15} photons/cm^2/s.

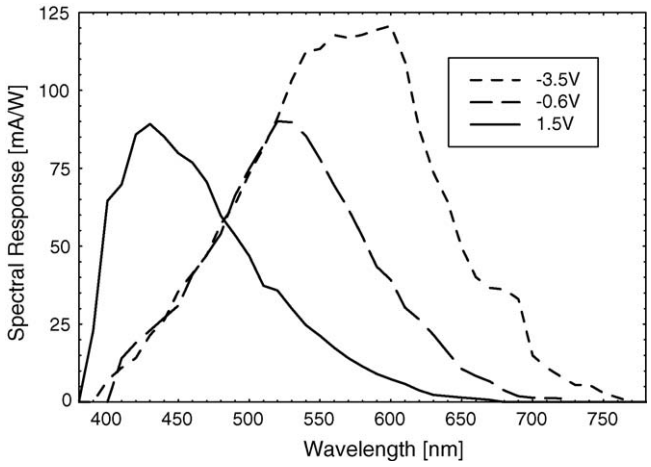

Fig. 6. Spectral response of the 'nipiin'-sensors for the applied bias voltages of $V = +1.5$, -0.6 and -3.5 V.

where ϕ_0 is the incoming photon flux, λ the wavelength of the incoming light and $\alpha(\lambda, x)$ is the absorption coefficient in the individual regions of the device. The wave propagation in the sensor stack was calculated by using the extinction coefficient of the individual layers. The generation rate was calculated for a photon flux of 10^{15} photons/cm^2/s. The influence of interference effects and reflections at the interfaces of the sensor stack were not considered in the calculations. Nevertheless, the simple calculation provides insights in the absorption behavior of the individual regions. The optical generation rate in the device structure for 450, 550 and 600 nm is given in Fig. 5.

The figure indicates that the optical generation rate for an incident wavelength of 450 nm is highest in region 'i_I'. The optical generation rate of blue light is distinctly reduced in regions 'i_{II}' and 'i_{III}' as almost all the light is absorbed in region 'i_I'. In region 'i_{II}' of the color sensor the optical generation is highest for an incoming wavelength of 550 nm. Red light with a wavelength of 600 nm is mainly absorbed in region 'i_{III}' of the sensor structure.

Applying a voltage to the color sensor leads to a variation of the spectral sensitivity. For positive applied voltages the top diode of the sensor is reverse biased and the bottom diode is forward biased. As a consequence the electric field in the top diode is increased. The schematic band diagram of the sensor for positive bias is shown in Fig. 4b. The photogenerated carriers in the top diode determine the overall photocurrent, whereas the photogenerated carriers in the bottom diode recombine. Therefore, the detector yields blue sensitivity. Changing the applied bias to a negative voltage leads to a forward biased top diode and a reverse biased bottom diode. In this case the sensor is green, respectively, red sensitive. For low negative voltages the electric field in region 'i_{II}' is much higher than the electric field in region 'i_{III}', so that the photocurrent is determined by the photogenerated carriers in region 'i_{II}' (Fig. 4c). This is achieved by inserting a very thin lightly doped 'n'-layer between the two absorption layers of the bottom diode. The thin lightly doped layer leads to an increased electric field in region 'i_{II}' of the bottom diode. Subsequently the band bending in this region 'i_{II}' of the device is stronger than the band bending in region 'i_{III}'. For higher negative voltages the electric field is enhanced throughout the entire bottom diode and the photocurrent is determined by the extracted carriers out of regions 'i_{II}' and 'i_{III}'. In this case the sensor exhibits green + red sensitivity (Fig. 4d).

3.2. Spectral sensitivity

The maximum of the spectral sensitivity of the 'nipiin'-structure shifts from red to green and blue due to a change of the bias voltage from $V = -3.5$ to +1.5 V. The spectral response of the 'nipiin'-sensor is shown in Fig. 6.

For a bias voltage of +1.5 V the sensor exhibits a maximum of the spectral sensitivity at a wavelength of 430 nm. Applying a negative bias to the optical sensor leads to the extraction of carriers out of the bottom diode. For a low negative voltage of -0.6 V the sensor exhibits green sensitivity. For low electric fields the photocurrent in the bottom diode is determined by the photogenerated carriers in region 'i_{II}'. The electric field in the bottom diode is not high enough to extract the photogenerated carriers out of region 'i_{III}'. The sensor exhibits a maximum of the spectral sensitivity for a wavelength of 550 nm. For high negative bias almost all carriers can be extracted out of regions 'i_{II}' and 'i_{III}' and the maximum of the spectral sensitivity shifts to 600 nm.

3.3. The image sensor

The pixel circuit of a sensor array is shown in Fig. 3. The charges created by the incoming light are stored by a pixel capacitor before being transferred to the readout circuit via the data line. A storage capacitor is required in each pixel as the sensor structure does not allow for operation in the charge storage mode.

Three chromatic images taken by the thin-film sensor array for different applied voltages are shown in Fig. 7a–7c.

The images correspond to the raw data taken by the sensor array. All three images have a resolution of 185 × 260 pixels. The images were taken for the applied bias voltages of -3.5, -0.6 and 1.5 V. Accordingly the sensor is red + green (Fig. 7a), green

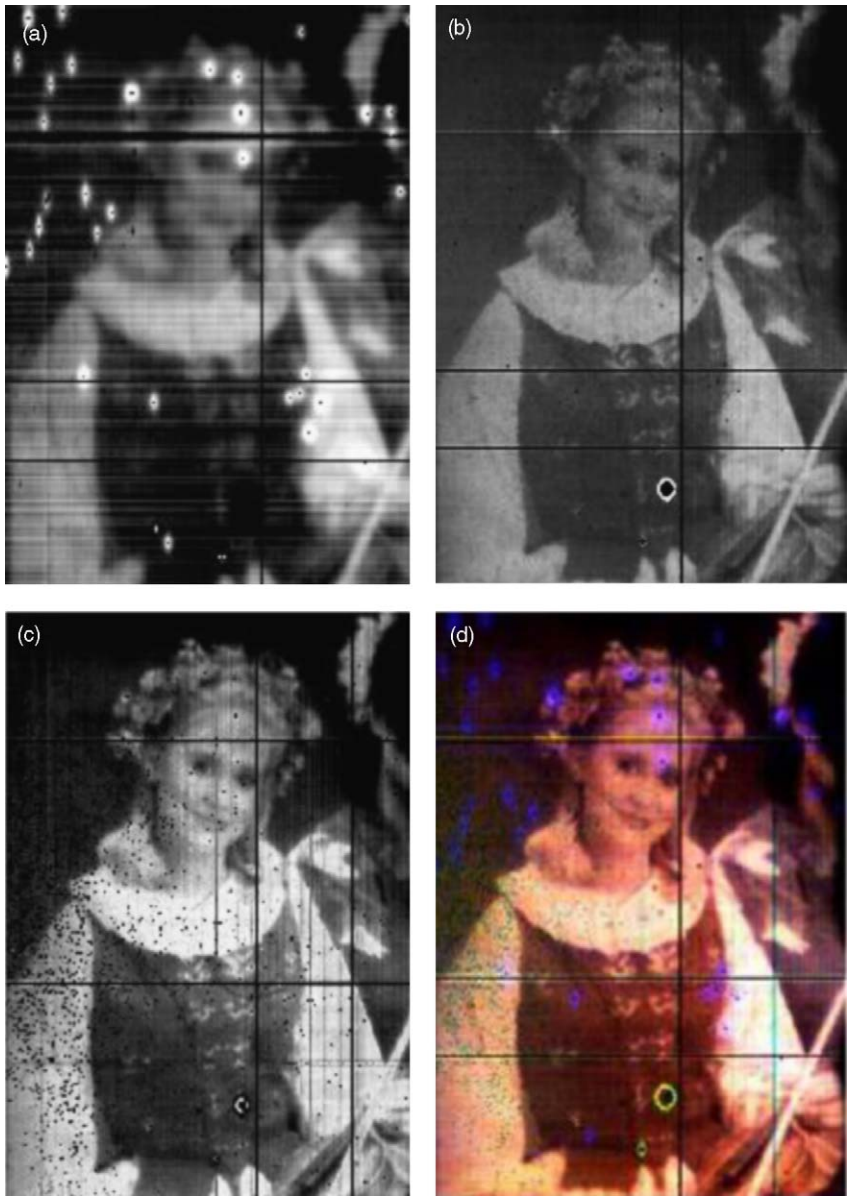

Fig. 7. Images taken for the applied bias voltages of: −3.5 V (a), −0.6 V (b) and +1.5 V (c). The images have a resolution of 185 × 260 pixels. A linear color transform was applied to merge the images in (a–c). The RGB image is given in (d).

(Fig. 7b) and blue (Fig. 7c) sensitive. A linear color transform was applied to merge the images in Fig. 7a–c. The RGB image is given in Fig. 7d.

4. Discussion

The quality of electronic images is influenced by several factors including the spatial resolution, the spectral resolution, the transient behavior of the sensor and noise. Conventional image sensors are limited by color moiré effects, which are observed for high spatial frequencies. The sensor structure presented here facilitates color moiré free imaging, due to a vertical stacking of the sensor channels.

In terms of the spatial resolution the image sensor is limited by pixel cross-talk. Only the back electrode and the 'n'-layer of the sensor were patterned. If now the senor array is exposed to light the electric field distribution in the 'nipiin'-structure is changed and neutral states in the vicinity of the 'p'-layer are recharged [17]. As a consequence the electric potential distribution within the device is changed. In particular the electric potential in the 'p'-layer is reduced due to the incident light. Therefore, inhomogeneous light exposure of the sensor leads to the formation of a potential gradient along the 'p'-layer. The potential gradient causes spreading of the photogenerated charges. Cross-talk and image spreading is mainly observed for the top diode. Hence, the contrast of the RGB image (Fig. 7d) is limited by the contrast of the top diode (Fig. 7c). A detailed description of the pixel cross-talk and image spreading is given in reference [18]. The pixel cross-talk can be reduced by patterning of the entire sensor stack. However, patterning of the sensor requires an additional deposition step as the gaps between the individual pixels have to be filled by an insulator. Otherwise the transparent conductive

oxide top contact cannot be prepared on top of the sensor stack. As an alternative only the 'p'-layer of the sensor could be patterned, whereas the 'i'-layers are unpatterened. By using such an approach the pixel cross-talk can be reduced and no additional deposition steps are needed.

The spectral sensitivity of the sensor array is another essential aspect in characterizing optical sensors. Colorimetric characterization of the sensor structures reveals color errors comparable with standard sensor arrays using optical filters. To achieve low colorimetric errors the spectral sensitivities of the three-color sensor have to be matched to the sensitivities of the colorimetric standard observer [15]. However, the spectral sensitivity of the individual channels depends on the design of the stacked sensor and the optoelectronic properties of the thin films. For example, a modification of the blue sensitivity of the sensor will affect the green and red sensitivity of the device as the optical wave propagation in the sensor stack is modified. Therefore, the spectral sensitivity of all three-color channels has to be optimized simultaneously. Optical and colorimetric simulations reveal that the blue sensitivity is limited by the optical bandgap of the material in region 'i_I', whereas the green and red sensitivity is limited by the optoelectronic properties in the bottom diode.

5. Summary

For the first time a color moiré effect or color aliasing free large area sensor array was realized. The sensor array was fabricated on glass substrates with a resolution of 512×512 pixels. The optical sensor and the readout transistors of the sensor array were realized by amorphous silicon and its alloys at deposition temperature below 300 °C. The vertically integrated sensor array enables the color moiré free color detection. Accordingly, the complete color information can be detected at the same position of a sensor array without the aid of optical filters. The color detector based on the anti serial connection of two amorphous diodes.

The developed large area sensor arrays are of particular interest for applications, where the requirements in terms of cost and scalability are different from classical microelectronics. Interesting applications areas are biochips and Lab-on-Chip systems.

Acknowledgments

The authors like to thank B. Rech, F. Finger and their research groups at the Research Center Jülich for their support in preparing the color sensors and the team of the process line at the Palo Alto Research Center for providing the TFT backplane.

References

[1] R.F. Lyon, P.M. Hubel, Eyeing the camera: into the next century, in: 10th Color Imaging Conference: Color Science and Engineering Systems, Technologies, Applications, Scottsdale, Arizona, November 2002.
[2] R.B. Mirell, Color separation in an active pixel cell imaging array using a triple-well-structure, United States Patent 5,965,865 (1999).
[3] P. Seitz, D. Leipold, J. Kramer, J.M. Raynor, Smart optical and image sensors fabricated with industrial CMOS/CCD semiconductor processes, SPIE 1900 (1993) 21.
[4] D.P. Poenar, R.F. Wolfenbuttel, Thin-film optical sensors with silicon compatible materials, Appl. Opt. 36 (21) (1997) 5109.
[5] H. Stiebig, J. Giehl, D. Knipp, P. Rieve, M. Böhm, Amorphous silicon three color detector, Mater. Res. Soc. Symp. Proc. 377 (1995) 517.
[6] K. Eberhardt, T. Neidlinger, M. Schubert, Three color sensor based on amorphous nipin layer sequence, IEEE Trans. Electron Devices 42 (1995) 1763.
[7] J. Zimmer, D. Knipp, H. Stiebig, H. Wagner, Amorphous silicon based unipolar detector for color recognition, IEEE Trans. Electron Devices 45 (5) (1999) 884.
[8] P. Rieve, M. Sommer, M. Wagner, K. Seibel, M. Böhm, a-Si:H color imagers and colorimetry, J. Non Cryst. Solids 266–269 (2000) 1168–1172.
[9] D. Knipp, H. Stiebig, J. Fölsch, F. Finger, H. Wagner, Amorphous silicon based nipiin structure for color detection, J. Appl. Phys. 83 (3) (1998) 1463.
[10] F. Palma, in: R.A. Street (Ed.), Multilayer Color Detectors, Springer Series in Material Science, vol. 37, Springer, Berlin, 2000, pp. 306–338.
[11] B. Schneider, P. Rieve, M. Böhm, Image Sensors in TFA (Thin Film on ASIC) Technology, Handbook of Computer Vision and Applications, Academic Press, Boston, 1998.
[12] J.A. Theil, Stacked multiple photosensor structure including independent electrical connections to each photosensor, United States Patent 6,373,117 (2002).
[13] R.A. Street, in: R.A. Street (Ed.), Large Area Image Sensor Arrays, Springer Series in Material Science, vol. 37, Springer, Berlin, 2000.
[14] O. Kluth, A. Löffl, S. Wieder, C. Beneking, L. Houben, B. Rech, H. Wagner, S. Waser, J.A. Selvan, H. Keppner, Texture etched Al-doped ZnO: a new material for enhanced light trapping in thin film solar cells, in: Proceedings of the 26th IEEE PVSEC, 1997, pp. 715–718.
[15] G. Wyszecki, W.S. Stiles, Color Science, John Wiley & Sons, USA, 1982.
[16] W. Luft, Y. Tuso, Hydrogenated Amorphous Silicon Alloy Deposition Processes, Marcel Dekker, Inc., 1993.
[17] B. Stannowski, H. Stiebig, D. Knipp, H. Wagner, Transient photocurrent of three-color detectors based on amorphous silicon, J. Appl. Phys. 85 (7) (1999) 3904.
[18] D. Knipp, R.A. Street, H. Stiebig, M. Krause, J.-P. Lu, S. Ready, J. Ho, in press.

Biographies

Dietmar Knipp received his master and doctoral degree in electrical engineering from the University Siegen, and Technical University Aachen (RWTH), Germany, in 1995 and 1999. From 1996 to 2000, he was with the Research Center Jülich first as research assistant, followed by the position of a postdoctoral scientist working on amorphous and nanocrystalline silicon and its application for optical sensors. From 2000 to 2002 he was with the Palo Alto Research Center Inc., USA, where he carried out research on organic and molecular electronics. Until joining the International University Bremen (IUB) as an assistant professor of electrical engineering in 2003, he was senior researcher at the Interuniversity Microelectronic Center (IMEC) in Leuven, Belgium, working in the area of Advanced Components and Sensor Systems. The research of Dietmar Knipp focuses on electronic devices and photonics, with particular emphasis on organic and molecular transistors, nanophotonics and optical sensor technologies.

Helmut Stiebig received the PhD degree in electrical engineering from the Aachen University of Technology, Aachen, Germany, in 1997. Since 1992, he has been with the Research Center Jülich, Institute of Photovoltaics, Jülich, Germany. He is currently the head of the research group "device analysis and sensor technology". His research interests include the investigation of the optoelectronic properties of amorphous and microcrystalline silicon and related materials, development of innovative device structures for solar cell applications, device analysis and numerical modeling, and the development of optical sensors based on thin-film technology.